Cooperative Infrastructure-based Vehicle Positioning

Fabian de Ponte Müller, Estefanía Munoz Diaz & Ibrahim Rashdan
German Aerospace Center - DLR
Institute of Communications and Navigation
Wessling, Germany
Email: fabian.pontemueller@dlr.de

***Abstract*—Many Advanced Driver Assistance Systems rely on an accurate self-localization. This is usually provided by Global Navigation Satellite Systems (GNSS) along with on-board sensors, such as inertial sensors, speed sensors, wheel-tick sensors and steering wheel angle sensors. However, this approach suffers from incremental error growth when long GNSS outages occur. Additionally, it is widely accepted that GNSS has a poor performance in urban-like environments due to satellite line-of-sight blockage, signal attenuation and multipath propagation. We propose a solution in which the error associated to GNSS-based positioning is contained by using surrounding road infrastructure objects (RIO) that are detected with a radar sensor. Since the position of these objects is a-priori not known, we suggest to share their estimated location among the vehicles using vehicle-to-vehicle communication and, in this way, improve their overall position accuracy over time. In this way, vehicles entering a GNSS-denied area are able to maintain their position accuracy, achieving even better results as if GNSS was available in the area of interest.**

I. Introduction

Road vehicles require an increasingly accurate and reliable estimation of their own position. Specially in the context of future Advanced Driver Assistance Systems (ADAS), as for instance collision avoidance or cooperative adaptive cruise control, this position estimation has to be robust to surrounding environmental changes. Self-positioning for road vehicles has been traditionally tackled using Global Navigation Satellite System (GNSS). This system allows a vehicle to localize itself on the Earth by measuring the propagation time of signals sent from at least four satellites. However, when obstacles block the Line-of-Sight (LoS) to the satellite, drops in signal power or complete satellite blockage lead to large errors in the estimated position. Also multipath propagation, especially in urban environments, are the cause of errors of several meters in the position of the vehicle. GNSS-alone positioning has also the drawback, that no position solution is available while driving through tunnels or inside garages and parking lots. Fig. 1 shows the estimated vehicle position for a drive through an urban canyon and exiting a tunnel. An epoch-wise least-squares algorithm (yellow) and a Kalman filter position estimation (blue) exhibit large errors in the order of several tens of meters in these situations or are at times completely unavailable.

To overcome this limitation and still provide a position solution, sensor fusion approaches are usually applied. These methods make use of on-board sensors like accelerometers, gyroscopes, speed sensors and odometers to estimate the position of the vehicle over time by following an approach known as dead-reckoning. This, however, has the drawback that errors in the sensors propagate to the position and accumulate over time. One possible approach to still provide localization in situations without GNSS is known as piloting. In piloting, the position of the vehicle is estimated by using external references or anchor points, called landmarks. These can be surrounding objects detected with a camera, radar sensor or laser scanner or radio beacons like mobile base stations or WiFi access points. In GNSS, the satellites orbiting the Earth can be considered as anchor points for localization.

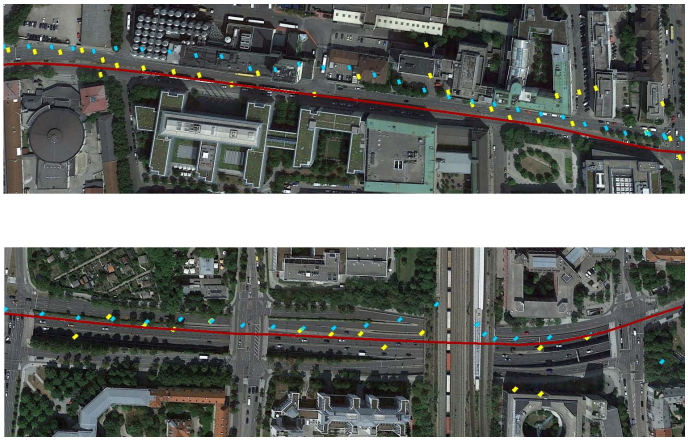

Fig. 1: The upper figure shows the drive through an urban canyon, while the bottom figure is a drive after exiting a tunnel and passing under two bridges. The true trajectory (red) can be compared to a GNSS epoch-wise position estimation (yellow) and a GNNS Kalman filter solution (blue).

When the location of surrounding landmarks, i.e. the map, is not a-priori known, an approach known as Simultaneous Localization and Mapping (SLAM) is followed [1]. In SLAM, the map of the environment is built at the same time as the robot, i.e. the vehicle, is localized. However, also in SLAM the same error accumulation earlier mentioned happens. Revisiting already detected landmarks, also known as loop-closure, helps to reduce this error growth.

Probabilistic maps in automotive environments for automated driving are presented in [2] and [3]. In [4], a localization algorithm for vehicles using off-the-shelf cameras and radar detecting lane markings and guard rails is proposed. A radar-based localization algorithm for a robot which assesses the

978-1-5090-1701-0/16/$31.00 ©2016 IEEE

quality of the generated maps is presented in [5]. The authors in [6] propose a SLAM approach only based on a 360° Frequency Modulated Continuous Wave (FMCW) 24 GHz radar in an automotive environment, whereas [7] use a laser scanner for the same purpose. The inherent drift of visual SLAM is backed by incorporating map information for vehicle self-localization in [8]. The authors in [9] propose a localization technique for rotating ranging sensors. In the railway domain, SLAM approaches based on track feature extraction have been proposed in [10].

In this paper, we propose a method for vehicle localization in areas where GNSS-positioning is either strongly corrupted due to blockage and multipath propagation or is even completely unavailable. For this purpose we adapt the SLAM approach based on automotive radar sensors to the special case of vehicle self-localization and extend it with a method in which the generated map of Road Infrastructure Objects (RIOs) is shared between vehicles in order to enhance their localization with each passing vehicle through this GNSS-denied area. To exchange this map, Vehicle-to-Vehicle (V2V) communication is considered. Dedicated Short-range Communication (DSRC) in the US and ITS-G5 in Europe are candidate technologies for direct inter-vehicle communication based on the IEEE 802.11 WiFi standard.

This paper is structured as follows: Section II proposes a Bayesian filter in which the vehicle position is estimated along with the location of the detected RIOs. The proposed method is evaluated in a simulated environment in Section III. The paper ends with the conclusions in Section IV.

II. Infrastructure Localization

In this section, the self-localization problem of one vehicle is formulated in a theoretical way, incorporating the measurement model of the radar sensor and the dynamic creation of a probabilistic map of RIOs.

A. Vehicle Localization

We consider that the vehicle estimates its position, forward speed and heading angle. For simplicity, in the frame of this work, it is assumed that the vehicle drives on a flat 2D surface and that the z-axis of the vehicle is aligned with the up-axis of the local navigation frame. Regarding the movement of the vehicle, we assume that it is only able to move in its longitudinal direction and that no vertical or side-wards motion exists. The resulting state vector is:

$$\mathbf{x}_k = \begin{bmatrix} x_k & y_k & v_k & \psi_k \end{bmatrix}, \tag{1}$$

where x_k and y_k are the coordinates of the vehicle in the 2D local navigation frame, v_k is the forward speed of the vehicle and ψ_k is the heading angle of the vehicle in relation to the local navigation frame. The state vector $\mathbf{x}_k$ has an associated variance-covariance matrix $\mathbf{P}_k$ which models its current uncertainty. We assume that the vehicle is equipped with a speed sensor and a gyroscope in order to estimate its own position when GNSS is not available. The prediction stage is given by the following equations:

$$x_{k+1} = x_k + \tau \cdot \hat{v}_k \cdot \cos(\psi_k), \tag{2}$$

$$y_{k+1} = y_k + \tau \cdot \hat{v}_k \cdot \sin(\psi_k), \tag{3}$$

$$v_{k+1} = \hat{v}_k + \nu_{\mathrm{v}}, \tag{4}$$

$$\psi_{k+1} = \psi_k + \tau \cdot (\hat{\omega}_k + \nu_\omega). \tag{5}$$

where τ is the prediction time step, $\hat{v}_k$ is the speed measurement from the speed sensor and $\hat{\omega}_k$ is the turn rate measurement from the z-axis gyroscope of the vehicle. The speed and the gyroscope measurements are corrupted with additive white Gaussian noise ν_{v} and ν_ω with standard deviations σ_{v} and σ_ω, respectively. The integrative nature of the prediction equations, yields an ever increasing error in the position coordinates x_k and y_k. When the non-linear prediction equations have to be linearized to compute the new variance-covariance $\mathbf{P}_{k+1}$ the implementation is known as an Extended Kalman Filter.

It will be considered that the vehicle is equipped with a GNSS receiver, which gives measurements of its position and velocity. A GNSS receiver estimates its 3D position by measuring the range towards a set of GNSS satellites and estimating its own clock bias at the same time. The 3D velocity is estimated in a similar way by measuring the Doppler shift to each satellite and solving the receiver clock drift. Out of the 3D velocity vector, the planar forward speed and the heading can be obtained. The models for the three measurements are given by:

$$\mathbf{p}_k^{\mathrm{GNSS}} = \mathbf{p}_k + \eta_{\mathrm{p}}, \tag{6}$$

$$v_{k+1}^{\mathrm{GNSS}} = v_k + \eta_{\mathrm{v}}, \tag{7}$$

$$\psi_{k+1}^{\mathrm{GNSS}} = \psi_k + \eta_\psi. \tag{8}$$

where the term on the left side are the GNSS-derived measurements for position, speed and heading and $\mathbf{p}_k = \begin{bmatrix} x_k & y_k \end{bmatrix}^\intercal$. The measurements are assumed to be corrupted by additive white Gaussian noise η_{p}, η_{v} and η_ψ.

B. Radar Targets

A radar sensor is able to measure the relative position and relative velocity of reflecting targets in its LoS. In vehicular environments, these measurements are usually given in the horizontal plane. In order to detect off-road objects, we consider a mid-range radar that has a larger opening angle around $\pm 30°$ and a detection range below 100 m. These radars are used for obstacle avoidance, in contrast to long-range radars used for automatic cruise control. Radars usually cluster several nearby reflectors in one target. At every measurement cycle, the list of detected targets is output. The radar target range and angle measurements have the following equation:

$$r_k^i = \sqrt{(R_{\mathrm{x}}^j - x_k)^2 + (R_{\mathrm{x}}^j - y_k)^2} + \eta_{\mathrm{r}}, \tag{9}$$

$$\theta_k^i = \mathrm{atan2}((R_{\mathrm{x}}^j - y_k), (R_{\mathrm{x}}^j - x_k)) - \psi_k + \eta_\theta, \tag{10}$$

where r_k^i and θ_k^i are the range and the angle of the i-th radar target measurement at time step k, R_{x}^j and R_{y}^j are the 2D coordinates of the j-th RIO, and η_{r} and η_θ are white

Gaussian noise. As a first step, in the scope of this work, we do not consider the target velocity measurements to enhance the vehicle's velocity and position estimation.

C. Infrastructure-based Localization

A RIO is any fixed object on the sides or above the road. These objects can be man-made structures like traffic signs, lamp posts or road gantries, as well as natural objects as trees or terrain. It is assumed that some of these objects will be capable of reflecting RF signals from a radar operating at typical mm-wave frequencies (77 GHz to 79 GHz). It is important that RIOs have a limited size in order to have an unambiguous location. Noise protection walls and road barriers are not suited structures as they are not limited to a single position but stretch over a wider space.

The self-positioning approach presented in this paper requires to filter out the static objects from the complete list of radar targets. This is assumed to be perfectly performed by using the forward speed of the vehicle. Moving objects erroneously detected as RIOs would introduce an error in the vehicle's self-localization. Further on, it is assumed that the static objects detected in the vicinity belong to a RIO. Parked vehicles or other semi-static objects do not provide a suited anchor point when using this method over longer periods of time. This cases are disregarded here.

For the purpose of vehicle self-positioning, the location of the RIOs has to be estimated along with the position of the vehicle. Hence, the state vector from Eq. 1 is extended with the position of J RIO coordinates:

$$\mathbf{x}_k = \begin{bmatrix} x_k & y_k & v_k & \psi_k & R^1_{\mathrm{x}} & R^1_{\mathrm{y}} \cdots R^J_{\mathrm{x}} & R^J_{\mathrm{y}} \end{bmatrix}. \quad (11)$$

At the beginning, the state vector contains only the first four states which belong to the vehicle. With new radar measurements, new RIOs are introduced into the state and its size is adapted dynamically. The first step after receiving a new radar measurement $\begin{bmatrix} r & \theta \end{bmatrix}^i_k$ is to check if the RIO is already included in the state vector. This is done by first computing an estimated measurement for each RIO contained in the state vector:

$$\hat{r}^j_k = \sqrt{(\hat{R}^j_{\mathrm{x}} - \hat{x}_k)^2 + (\hat{R}^j_{\mathrm{y}} - \hat{y}_k)^2}, \quad (12)$$

$$\hat{\theta}^j_k = \mathrm{atan2}((\hat{R}^j_{\mathrm{y}} - \hat{y}_k), (\hat{R}^j_{\mathrm{x}} - \hat{x}_k)) - \hat{\psi}_k, \quad (13)$$

and then by computing the Mahalanobis distance δ from the received measurement $\begin{bmatrix} r & \theta \end{bmatrix}^i_k$ to the estimated measurement $\begin{bmatrix} \hat{r} & \hat{\theta} \end{bmatrix}^j_k$ according to:

$$\delta^{i,j} = \begin{bmatrix} \hat{r}^j_k - r^i_k \\ \hat{\theta}^j_k - \theta^i_k \end{bmatrix} \cdot (\mathbf{P}_H + \mathbf{R})^{-1} \cdot \begin{bmatrix} \hat{r}^j_k - r^i_k \\ \hat{\theta}^j_k - \theta^i_k \end{bmatrix}^{\mathsf{T}}, \quad (14)$$

where $\mathbf{R}$ is the 2x2 covariance matrix modeling the errors of the radar range and angle measurements and $\mathbf{P}_H = \mathbf{H} \cdot \mathbf{P} \cdot \mathbf{H}^{\mathsf{T}}$, where $\mathbf{P}$ is the variance-covariance matrix of the state vector $\mathbf{x}$ and $\mathbf{H}$ is the Jacobian matrix of Eq. 12 and 13 with respect to the state vector $\mathbf{x}_k$. The Mahalanobis distance is specially suited since it takes the uncertainties in both, the current position and the radar measurements, into account. If the Mahalanobis distance is below a certain threshold, the radar measurement is considered to stem from the j-th RIO and a Bayesian update step is performed:

$$\mathbf{K} = \mathbf{P} \cdot \mathbf{H}^{\mathsf{T}} \cdot \mathbf{P}_H^{-1}, \quad (15)$$

$$\mathbf{x}_k = \mathbf{x}_k + \mathbf{K} \cdot \begin{bmatrix} \hat{r}^i_k - r^i_k & \hat{\theta}^i_k - \theta^i_k \end{bmatrix}^{\mathsf{T}}, \quad (16)$$

$$\mathbf{P}_k = (\mathbf{I} - \mathbf{K} \cdot \mathbf{H}) \cdot \mathbf{P}, \quad (17)$$

where $\mathbf{K}$ is the Kalman gain and $\mathbf{I}$ is a 2×2 identity matrix. In this way, besides updating the estimated self-position, the position of the rest of detected RIOs are subsequently corrected. If, however, the Mahalanobis distance exceeds the named threshold, the radar measurement is assumed to stem from a new unknown RIO. In this case, its position estimation

$$\hat{R}^j_{\mathrm{x}} = \hat{x}_k + r^i_k \cdot \cos(\hat{\theta}^i_k + \psi_k), \quad (18)$$

$$\hat{R}^j_{\mathrm{y}} = \hat{y}_k + r^i_k \cdot \sin(\hat{\theta}^i_k + \psi_k), \quad (19)$$

is included by extending the state vector $\mathbf{x}_k$. The association threshold value is a tuning parameter, which makes it possible to trade-in non-detections (if the threshold is too tight) for miss-associations (if the threshold is set too loose). The correct threshold also depends on the distance between neighboring RIOs, since nearby RIOs are more likely to be wrongly associated.

D. Cooperative Localization

Once the first vehicle traverses the GNSS-denied zone, the current RIO map, composed by the state vector

$$\mathbf{x}^R = \begin{bmatrix} R^1_{\mathrm{x}} & R^1_{\mathrm{y}} \cdots R^J_{\mathrm{x}} & R^J_{\mathrm{y}} \end{bmatrix} \quad (20)$$

and its associated variance-covariance sub-matrix $\mathbf{P}^R$, are exchanged in the Vehicular Ad-hoc Network (VANET). A second vehicle receiving this information, can initialize its state vector $\mathbf{x}$ and its variance-covariance matrix $\mathbf{P}$. Now, when this second vehicle has a new radar measurement available, it will perform the same measurement update step and either associate with an existing RIO or creating a new RIO, as described above.

For disseminating information in a VANET, suited routing protocols have been standardized in Europe by European Telecommunications Standards Institute (ETSI) [11]. Based on the Greedy Perimeter Stateless Routing algorithm, geographical-scoped broadcasts bring the map of RIOs inside so-called Decentralized Environmental Notification Messages (DENMs) from the exit to the entrance of the GNSS-denied area. This is done by transmitting the messages over several hops and, if no vehicle is available, by storing and forwarding the information when a suited neighbor vehicle comes into range. At the entrance of the GNSS-denied area the information is kept alive by re-broadcasting it. Inside DENMs, the data version field makes it possible to send updated information when a new vehicle has traversed the GNSS-denied area and updates the RIO map.

The amount of communication resources required to exchange the current RIO map is calculated next. Per RIO, two float values are required for its horizontal position. The

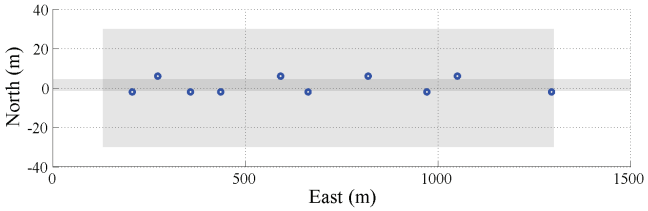

Fig. 2: Simulated road section with RIOs uniformly distributed on both sides of the road. Inside the gray shaded area GNSS is not available.

variance-covariance matrix increases quadratically with the number of RIOs. For instance, ten RIOs come along with a 10×10 variance-covariance matrix. We suggest coding one reference position with double precision and all RIO position coordinates and uncertainties with single precision values. For 10 RIOs, this results in 244 Byte payload, while 20 and 50 RIOs require 884 Byte and 5.2 kByte, respectively. Up to 26 RIO could be stored and transmitted in one V2V message, considering that its maximum payload length is 1536 Byte (disregarding network layer overhead). A Cooperative Awareness Message (CAM), for comparison, is between 300 and 500 Byte long.

III. Simulation Results

To demonstrate the functionality of the proposed vehicle self-positioning approach based on road infrastructure, a simulation environment has been developed. In Matlab, a vehicle drives on a straight section of road with infrastructure components uniformly distributed on both sides. Figure 2 shows the $1500\,\mathrm{m}$ road section and the distribution of 10 RIOs inside the GNSS-denied environment.

In the simulator, the true position, velocity and turn-rate of the vehicle were simulated at $1\,\mathrm{kHz}$. The GNSS receiver, the speed sensor, the gyroscope and the radar sensor have been modeled. Table I summarizes both, the simulator and the sensor parameters for this evaluation. The GNSS receiver has been modeled by adding white Gaussian noise on the true position of the vehicle. GNSS updates were generated at $5\,\mathrm{Hz}$. The speed sensor output longitudinal speed measurements at $5\,\mathrm{Hz}$, which were modeled by taking the magnitude of the velocity vector and adding white Gaussian noise. The z-axis gyroscope is also modeled by adding white Gaussian noise to the turn rate of the vehicle and is simulated at $100\,\mathrm{Hz}$. The radar measurements in range and angle are independent of each other and corrupted by white Gaussian noise. Every new vehicle that drives the loop is a new realization of the experiment. The plots in this section show representative realizations of the experiment.

A. First vehicle

The first test consists of one vehicle driving from the GNSS-available road section, to a GNSS-denied area and again out to the GNSS-available area. Fig. 3 shows the position error in blue and the 1σ position uncertainty in red. For comparison, in

TABLE I: Simulation parameters

Parameter	Value
Road section length	$1500\,\mathrm{m}$
GNSS position, speed, heading noise (1σ)	$5\,\mathrm{m}$, $0.3\,\mathrm{m\,s^{-1}}$, $0.5°$
Speed sensor noise (1σ)	$0.1\,\mathrm{m\,s^{-1}}$
Turn-rate sensor noise (1σ)	$1\,°\,\mathrm{s^{-1}}$
Radar range, angle noise (1σ)	$0.1\,\mathrm{m}$, $1°$
Radar range limit and angle of view	$50\,\mathrm{m}$, $25°$
Number of RIOs	10

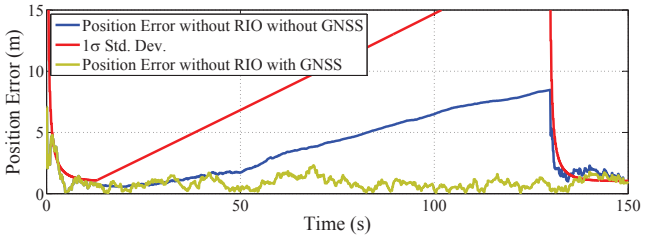

Fig. 3: The figure shows the position error (blue) and its uncertainty (red) when the vehicle drives through a GNSS-denied area between second 13 and 130. In yellow the position error if GNSS had been available is displayed for comparison.

yellow the position error if GNSS was available is displayed. It can be seen how the initial error quickly decreases when subsequent GNSS measurements become available. When the GNSS denied area is entered in second 13, the position estimation error grows with respect to the GNSS-available curve due to the integrative nature of the dead-reckoning method. Note that, thanks to the speed sensor, the integration of position errors is not as large as could be expected by double-integrating the accelerometer using a strap-down algorithm. The heading error will also grow due to the integration of the gyroscope noise. At the exit of the GNSS-denied area in second 130, GNSS measurements are again available and the position error decreases again to meet the green curve.

In the second test, the same vehicle (the same realization of vehicle sensors) activates its radar sensor and is able to detect surrounding RIOs. Fig. 4a shows the position error (green) and the 1σ position uncertainty (red). The error growth has slightly been contained and the position uncertainty stays constant while the radar has a RIO in its LoS. The sooner a RIO is detected inside the GNSS-denied zone the smaller is its associated uncertainty and its estimation error. This can be seen in Fig. 4b and 4c. It can also be noticed, how the error and the uncertainty of each of the RIO position estimations is clearly reduced when exiting the GNSS-denied area and re-acquiring a GNSS position fix. The latest acquired RIO profits most in terms of uncertainty and error.

B. Subsequent vehicles

The presented cooperative method is based on the principle that subsequent vehicles obtain the RIO position estimation of previous vehicles over V2V communication. Fig. 5 displays the vehicle position error, RIO error and uncertainty for the

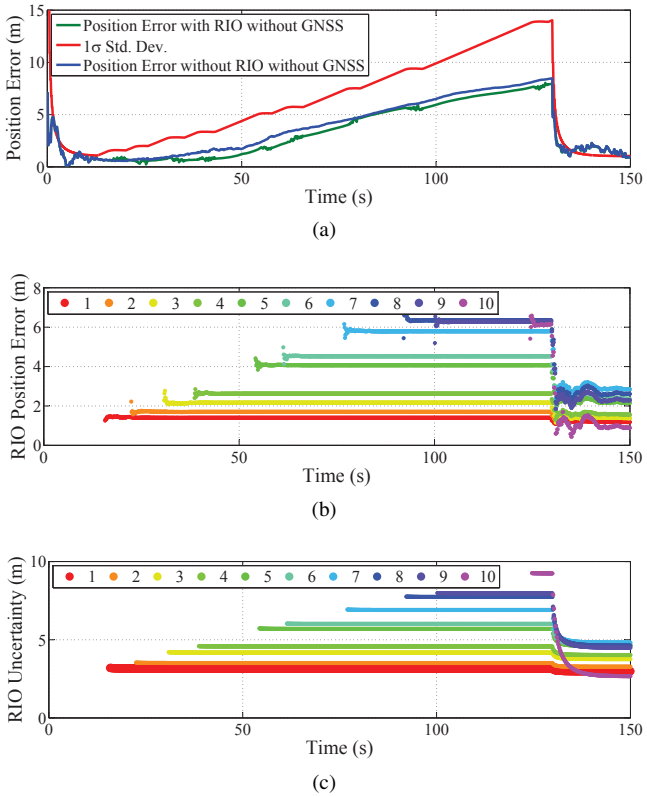

Fig. 4: First Vehicle - The upper figure shows the position error using RIO (green) and its uncertainty (red) when the vehicle drives through a GNSS-denied area. For comparison also the solution without RIO (blue) is displayed. The two bottom figures show the estimation error in the detected RIOs and its associated uncertainty.

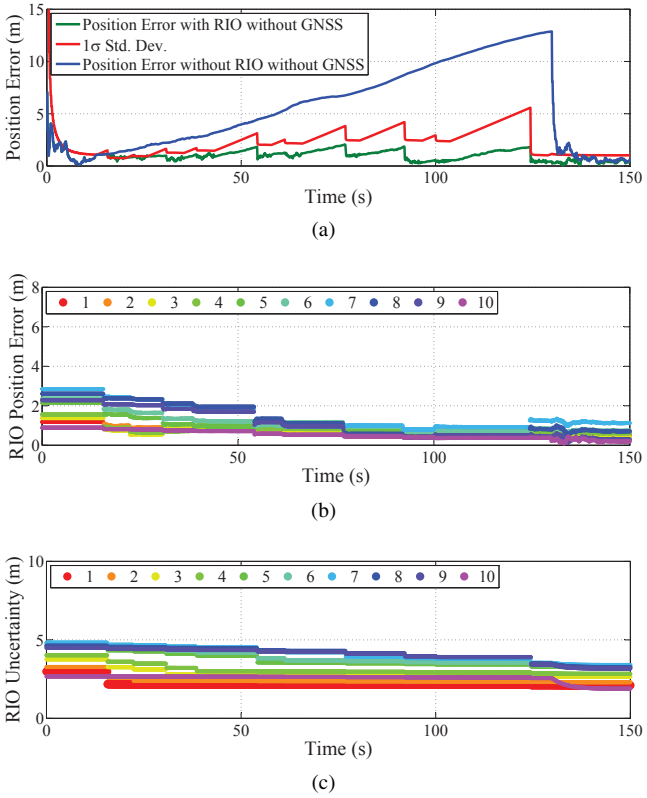

Fig. 5: 2nd Vehicle - The upper figure shows the position error using RIO (green) and its uncertainty (red) when the second vehicle drives through a GNSS-denied area. For comparison also the solution without using RIO (blue) is displayed. The bottom figure shows the estimation error in the detected RIOs and its associated uncertainty.

second vehicle. Fig. 5a compares the vehicle position using the RIO-supported self-positioning (green) and the prediction based solely on the on-board sensors (blue). Already in this realization an improvement in position accuracy can be seen. Unlike the first vehicle, the second vehicle enters the GNSS-denied area with a prior estimation of the RIO position that he received over V2V communication. This can be seen Fig. 5b and Fig. 5c. After exiting the GNSS-denied area, the uncertainty in the RIO position has been further decreased.

The improvement using the RIO-supported positioning increases the more vehicles have traversed the GNSS-denied area and the better the RIOs are estimated. With each run, the RIO uncertainty decreases and the RIO position estimation stabilizes. Fig. 6 shows the vehicle position and RIO estimation of the 10-th vehicle driving through the GNSS-denied zone. In Fig. 6a, the benefit of having a more accurate map gets clear. For comparison, the position error curve with GNSS activated has been included. It can be seen, how the RIO-based self-positioning (green) has an error in the order of what can be expected if GNSS had been available (yellow). The RIO position error has further decreased to less than $1\,\mathrm{m}$ (see Fig. 6b). Actually, the vehicle positioning error is related to the RIO position error when in detection range of the RIO. With increasing number of RIO objects, the vehicle positioning error can further be decreased on the expense of higher communication resources.

IV. Conclusions

In this paper, a new method for cooperative vehicle self-positioning for road sections where GNSS is either not available or corrupted with large errors due to e.g. multipath propagation is proposed. The growth of the position error while driving in these environments is limited by using a radar sensor which is able to detect and track surrounding road infrastructure objects (RIO). The first vehicle creates a probabilistic map of the location of RIOs and shares this over V2V communication with subsequent vehicles. We have shown in a simulation environment how the map of RIOs is enhanced over time and how its incorporation into the vehicle's self-positioning algorithm makes it possible to maintain a position accuracy in the order of that expected with GNSS. The next step will be to evaluate the proposed method in real road environments with real sensors.

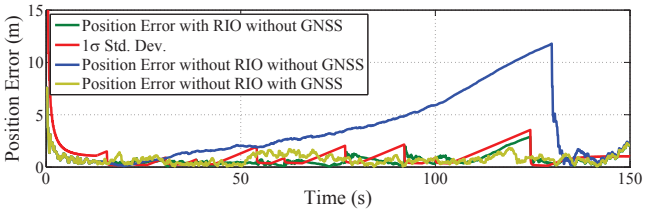

(a)

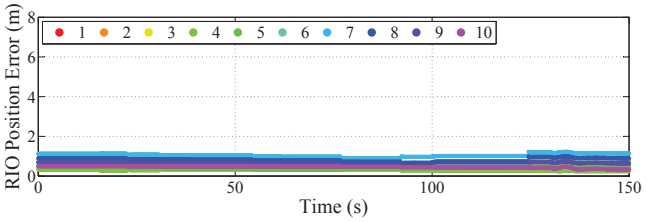

(b)

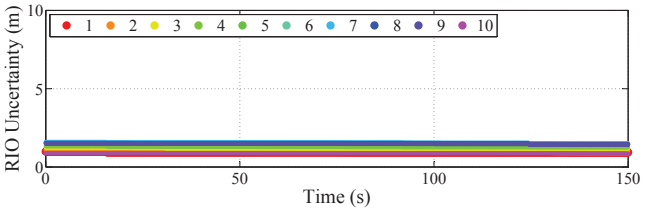

(c)

Fig. 6: 10th Vehicle - The upper figure shows the position error using RIO (blue) and its uncertainty (red) when the 10th vehicle drives through a GNSS-denied area. For comparison also the solution without RIO (green) and the solution if GNSS had been available (yellow) are displayed. The bottom figure shows the estimation error in the detected RIOs and its associated uncertainty.

REFERENCES

[1] S. Thrun, W. Burgard, and D. Fox, "A probabilistic approach to concurrent mapping and localization for mobile robots," *Autonomous Robots*, vol. 5, no. 3-4, pp. 253–271, 1998.

[2] J. Levinson and S. Thrun, "Robust vehicle localization in urban environments using probabilistic maps," in *Robotics and Automation (ICRA), 2010 IEEE International Conference on*. IEEE, 2010, pp. 4372–4378.

[3] J. Levinson, M. Montemerlo, and S. Thrun, "Map-based precision vehicle localization in urban environments." in *Robotics: Science and Systems*, vol. 4. Citeseer, 2007, p. 1.

[4] M. Lundgren, E. Stenborg, L. Svensson, and L. Hammarstrand, "Vehicle self-localization using off-the-shelf sensors and a detailed map," in *Intelligent Vehicles Symposium Proceedings, 2014 IEEE*. IEEE, 2014, pp. 522–528.

[5] M. Chandran and P. Newman, "Motion estimation from map quality with millimeter wave radar," in *Intelligent Robots and Systems, 2006 IEEE/RSJ International Conference on*. IEEE, 2006, pp. 808–813.

[6] R. Rouveure, P. Checchin, P. Faure, M.-O. Monod, and L. Trassoudaine, "Simultaneous localization and map building using radar sensor in extensive outdoor environment: First results," in *Proceedings of 1rst Workshop on Planning, Perception and Navigation for Intelligent Vehicles IEEE ICRA*, 2007, pp. 808–813.

[7] M. Yang, C. Wang, H. Fang, and B. Wang, "Laser radar based vehicle localization in gps signal blocked areas," *International Journal of Computational Intelligence Systems*, vol. 4, no. 6, pp. 1100–1109, 2011.

[8] G. Floros, B. van der Zander, and B. Leibe, "OpenStreetSLAM: Global vehicle localization using OpenStreetMaps," in *Proceedings of the IEEE International Conference on Robotics and Automation (ICRA)*. IEEE, 2013, pp. 1054–1059.

[9] D. Vivet, P. Checchin, and R. Chapuis, "Radar-only localization and mapping for ground vehicle at high speed and for riverside boat," in *Robotics and Automation (ICRA), 2012 IEEE International Conference on*, May 2012, pp. 2618–2624.

[10] O. Heirich, P. Robertson, and T. Strang, "Railslam-localization of rail vehicles and mapping of geometric railway tracks," in *Robotics and Automation (ICRA), 2013 IEEE International Conference on*. IEEE, 2013, pp. 5212–5219.

[11] *ETSI TS 102 636-4-1 Intelligent Transport Systems (ITS); Vehicular communications; GeoNetworking; Part 4: Geographical addressing and forwarding for point-to-point and point-to-multipoint communications; Sub-part 1: Media-Independent Functionality*, European Telecommunications Standards Institute (ETSI) Std.